Electron Delocalization and Electrostatic Repulsion at the Origin of the Strong Spin Coupling in Mixed-Valence Keggin Polyoxometalates: Ab Initio Calculations of the One- and Two-Electron Processes

Nicolas Suaud,*[a, b] Alejandro Gaita-Ariño,[a] Juan Modesto Clemente-Juan,[a] and Eugenio Coronado*[a]

Abstract: We present here a general theoretical procedure to treat the problem of electron delocalization and magnetic interactions in high-nuclearity mixed valence clusters based on polyoxometalates. The main interactions between the delocalized electrons of mixed-valence polyoxometalate anions are extracted from valence spectroscopy ab initio calculations on embedded fragments. Electron transfer, magnetic coupling and exchange transfer parameters between nearest and next-nearest-neighbor metal ions, as well as the value of the electrostatic repulsion between pairs of metal ions are determined. These parameters are introduced in a model Hamiltonian that considers the whole anion. It thus provides macroscopic properties that should be compared with the experimental data. This method is applied to a two-electron-reduced polyoxowolframate Keggin anion. The results demonstrate that the electron transfer processes, combined with the Coulombic repulsion between the "extra" electrons, induce a strong antiferromagnetic coupling between the two delocalized spins providing a definite explanation of the diamagnetic properties of these high nuclearity mixed-valence clusters.

Keywords: ab initio calculations · magnetic properties · mixed-valent compounds · polyoxometalates

Introduction

Polyoxometalates[1] (POM) are an appealing class of inorganic compounds not only for synthetic chemists, who build amazing cluster structures[2] and find an ever-growing number of applications,[3] but also for theoreticians who have found in POM excellent molecular models for the study of a wide range of electronic structures. Indeed, POMs can act as ligands encapsulating paramagnetic transition metal ions;[4] they are also electron acceptors that can be reduced giving rise to large mixed valence clusters ("heteropoly blues" and "heteropoly browns"). Furthermore, the large number of structurally-related polyoxoanions, together with the chemical control of their nuclearity and of the angles and distances between the metal centers, make POM ideal objects for a detailed study of the electronic and magnetic interactions at the molecular level.

Model Hamiltonians (Heisenberg,[5] t–J,[6] Hubbard[7] or Pariser–Parr–Pople[8]) are extremely useful tools that allow to link macroscopic properties (magnetic susceptibility, specific heat) to microscopic parameters (electron transfer, magnetic coupling, electrostatic repulsion etc.).

However, most of mixed-valence POMs are by far too complex and a fitting of the experimental data to a theoretical model based on these effective Hamiltonians is clearly insufficient to provide reliable values of these parameters. Some of these systems were treated with DFT methods[9] but their size prevents any Configuration Interaction (CI) ab initio calculation to be performed on the whole cluster.

The aim of the present paper is to prove the efficiency of a hybrid approach that combines model Hamiltonians performed on the whole cluster with ab initio calculations of the microscopic parameters performed on embedded fragments of POM. For that purpose, we chose the appealing case of a two-electron-reduced polyoxowolframate anion of Keggin structure as a testing ground for this procedure. A previous work[10] proved that very accurate values of the

[a] Dr. N. Suaud, A. Gaita-Ariño, Dr. J. M. Clemente-Juan, Prof. E. Coronado
Instituto de Ciencia Molecular, Universidad de Valencia
C/Doctor Moliner 50, 46100 Burjassot (Spain)
Fax: (+34) 963544859
E-mail: Nicolas.Suaud@irsamc.ups-tlse.fr
Eugenio.Coronado@uv.es

[b] Dr. N. Suaud
IRSAMC, Laboratoire de Physique Quantique
Université Paul Sabatier
118 route de Narbonne, 31062 Toulouse Cedex (France)
Fax: (+33) 561557694

 DOI: 10.1002/chem.200305628

electron transfer parameters can be obtained from calculations on corner-sharing WO_5 pyramids embedded in a correct bath that models the main effects of the rest of the crystal. It also allowed to rationalize to some point the diamagnetism of the Keggin anion reduced by two electrons. In view of these interesting results, the present work goes further and determines all the main microscopic parameters acting in the two-electron reduced Keggin polyoxotungstate structure. These parameters are then introduced in a Hubbard-type Hamiltonian and the macroscopic properties of the mixed-valence cluster are derived. Such a procedure allows us to present a coherent view of the diamagnetic properties of this compound through a deeper understanding of the role of the microscopic interactions of the pair of delocalized "extra" electrons injected by the reduction process.

In the next Section, the first subsection presents the principles of extraction of the microscopic parameters from embedded fragment calculations. The two types of fragments used in this work are also described: a 4W-based fragment permits to evaluate *simultaneously* the interactions between the two types of nearest-neighbors and the next-nearest-neighbors metal centers; 2W-based fragments allow the *independent* evaluation of the interactions between all pairs of metal centers. The second subsection provides an overview of the model Hamiltonians used in this paper and of the way to extract the value of their parameters from ab initio calculations. The subsequent Section is then devoted to present the results obtained from CASSCF, CASPT2, MONO, DDCI2 and DDCI ab initio methods described in the Computational Details. Finally, in following Section, these interactions are introduced as parameters of the Hubbard model Hamiltonian that describes the whole Keggin anion. It thus allows to revisit and rationalize the experimental diamagnetism observed in the two-electron reduced polyoxotungstate Keggin anions.

Abstract in French: *Cet article détaille une procédure générale qui associe l'évaluation de paramètres microscopiques et la prédiction de propriétés macroscopiques. Les principales interactions entre les électrons délocalisés sur des polyoxométalates à valence mixte sont extraites à partir du calcul de la spectroscopie de valence de fragments immergés dans un bain qui reproduit les principaux effets du reste du cristal sur le fragment considéré. Nous avons extrait non seulement la valeur du transfert électronique, du couplage magnétique et du paramètre de "exchange-transfer" entre ions métalliques premiers et seconds voisins, mais encore la valeur de la répulsion électrostatique entre les électrons délocalisés. Ces valeurs ont été introduites comme paramètre d'un Hamiltonien modèle qui décrit le polyoxométalate dans son ensemble. Les résultats fournis par cet Hamiltonien sont alors directement comparables aux résultats expérimentaux. Cette méthode a été appliquée au cas d'un polyoxotungsténate de type Keggin réduit par deux électrons. Nous avons alors pu montrer que le transfert électronique induit un très fort couplage antiferromagnétique entre les deux électrons délocalisés alors que les processus de super-échange n'ont aucun effet sur ce couplage. Le très grand écart d'énergie qui en découle entre le singulet fondamental et le premier état triplet excité permet une explication définitive des propriétés diamagnétiques de tels composés à valence mixte.*

Theoretical Models

Embedded fragment calculations: Fragment spectroscopy calculation is a widely used method that provides accurate evaluations of the intensity of microscopic parameters between metal centers of strongly correlated materials. It consists of ab initio[11,12] or DFT[13] treatments of the interactions acting between the electrons and nuclei of a small fragment of the crystal. This fragment is embedded in a bath of punctual charges and total ion pseudopotentials (TIPs)[14] adapted to reproduce the main effects of the rest of the crystal, namely, the short-range Pauli exclusion and the long-range Madelung potential. A correct modeling of these effects is crucial for an accurate evaluation of the interactions, particularly of the magnetic coupling.[15]

The embedding (see Figure 1) is obtained by replacing the atoms surrounding the ab initio considered fragment by punctual charges. It includes the remaining ions in the central Keggin complex, as well as several shells of Keggin polyoxocomplexes and the corresponding hydronium countercations. Its shape (which respects the local symmetry of the compound), its size (larger than 20 Å from the center of the fragments, it contains more than 1200 punctual charges) and the values of the punctual charges permit to reach an accurate enough modeling of the Madelung field.[10,11,16] TIPs are added to the charges modeling all the atoms of the first and second shells enclosing the fragment under consideration (about 150 centers). They allow for avoiding an excessive polarisation of the anions of the fragment toward the punctual positive charges. Evidences of the accuracy of the punctual charges and TIPs to reproduce the main effects of the rest of the crystal on the fragments are presented in second Section in the Results and Discussion.

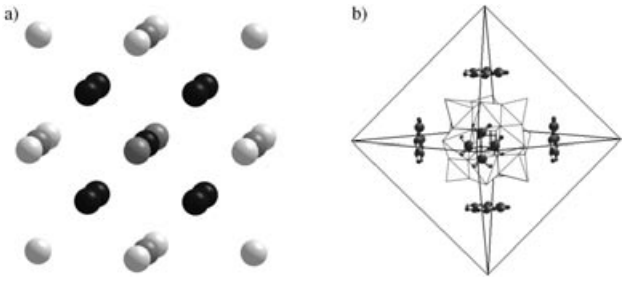

Figure 1. Embedding of punctual charges and TIPs designed to reproduce the main effects of the rest of the crystal on the fragments used to calculate the microscopic interaction between W centers. a) Keggin anions considered in the embedding. Around the central anion, there is a cube, then a octahedron, both at approximately 12 Å, and at around 18 Å from the center we can see a cuboctahedron. b) Position of the countercations relative to the Keggin anions.

The embedded fragments used in this work are of two kinds, one 4W-based fragment (tetramer W_4O_{16}) and five 2W-based fragments. The W_4O_{16} fragment contains four corner-sharing WO_5 pyramids. It allows the simultaneous evaluation of the interactions between corner-sharing, edge-sharing and next-nearest-neighbors (*nnn*) W metallic centers. It is represented in Figure 2 where the atoms denoted as W_1 and W_2 belong to the same triad of edge-sharing WO_6 octahedra. The pair W_3–W_4 is equivalent to W_1–W_2 and belongs to a triad adjacent to the triad supporting W_1 and W_2. W_1 and W_4 belong to corner-sharing octahedra, as do the equivalent pair W_2 and W_3. One can notice that the fragment do not include the sixth oxo anions of the W atom coordination sphere, the oxo anions that belongs the encapsulated PO_4 clathrate. Indeed, it has been shown that these anions do not support any important pathway for the delocalization of the unpaired electrons between nearest and next-nearest-neighbors W ions and their effects can be accurately reproduced by punctual charges and TIPs.[10] Three dimer fragments, based on two WO_5 pyramids, model the pairs of W atoms separated by distances $d_{III}=5.2$, $d_{IV}=3.8$, and $d_V=3.5$ Å. They permit an independent evaluation of the interactions between nearest (distances d_{IV} and d_V) and next-nearest-neighbors (distance d_{III}) W atoms, respectively. They provide a cross-checking of the results obtained from the 4W-based fragment and their smaller sizes allow much quicker calculations. They are represented in Figure 3. Two W_2O_9 fragments correspond to corner sharing (fragment containing W_1 and W_4, distance d_{IV}) and edge-sharing (fragment containing W_1 and W_2, distance d_V) WO_6 octahedra. A W_2O_{10} fragment (based on W_1 and W_3) corresponds to *nnn* WO_6 octahedra. The W and O ions that pertain to the 4W-based fragment but not to these dimer fragments are modeled by punctual charges and TIPs and added to the embedding. The accuracy of such a simplification is discussed in the second Section of the Results and Discussion. Two PW_2O_{14} fragments permit to evaluate the electrostatic repulsion between the delocalised electrons when they are located on W ions separated by a distance $d_I=7.3$ or $d_{II}=6.3$ Å. They contain the two W atoms, the O ions of their coordination sphere and the atoms of the PO_4 clathrate encapsulated in the Keggin anion.

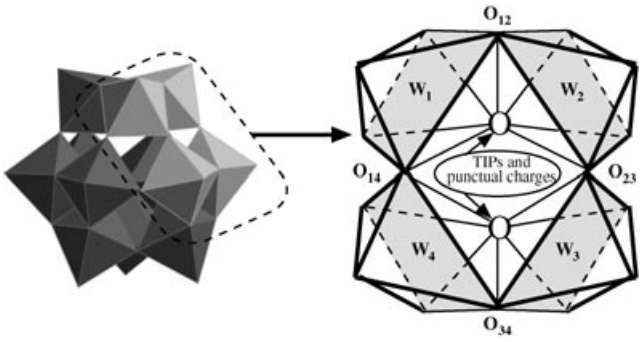

Figure 2. $\alpha PW_{12}O_{40}$ Keggin anion and the W_4O_{16} fragment. The oxygen atoms occupy the corners of the pyramids. W_1 and W_2 pertain to edge-sharing WO_6 octahedra, W_1 and W_4 pertain to corner-sharing WO_6 octahedra. For clarity reasons, only the O shared by the WO_6 octahedra and the PO_4 encapsulated clathrate, modeled by punctual charges and TIPs, has been represented. The other atoms modeled by punctual charges and TIPs are not represented.

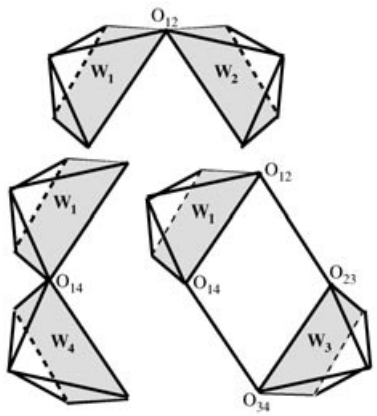

Figure 3. Three 2W-based fragments. The oxygen atoms occupy the corners of the pyramids. The notations for the W atoms correspond to those of Figure 2. Atoms modeled by punctual charges and TIPs are not represented.

All the atomic coordinates are extracted from the structure of the Keggin anion determined by X-ray crystallographic study of the $(H_5O_2^+)_3$ $(PW_{12}O_{40}^{3-})$ salts.[17] The tetrahedric symmetry of this compound induces the equivalence of all the W atoms and of the interactions $W_1 \leftrightarrow W_2$ and $W_3 \leftrightarrow W_4$ (along edge-sharing octahedra) as well as the interactions $W_1 \leftrightarrow W_4$ and $W_2 \leftrightarrow W_3$ (along corner-sharing octahedra) and of the interaction $W_1 \leftrightarrow W_3$ and $W_2 \leftrightarrow W_4$ between *nnn*. This permits much quicker calculations, reduces the number of independent parameters and thus highly simplifies the model Hamiltonians used to describe the behavior of the systems.

Model Hamiltonians and evaluation of their parameters: In magnetic compounds only a few electrons are responsible for the macroscopic properties. They usually belong to open-shell orbitals and are localized energetically near the Fermi level. The effect of those electrons that are not explicitly treated in the model are taken into account effectively, that is in the value of the interactions between the model electrons. It is thus of the highest interest to rely on model Hamiltonians based on a reduced number of electrons interacting through effective parameters. The space of determinants or configurations on which the model Hamiltonian is based is called the model space; the other determinants or configurations form the outer-space. The extended Hubbard[7] Hamiltonian is the most complex model frequently used to describe the behavior of mixed-valence compounds. The model space is based on all the determinants formed by spanning all the model electrons onto all the orbitals that are taken into account. It considers the orbital energies, electron transfer (hopping) integrals, the on-site electrostatic repulsion and the inter-site electrostatic repulsion (between electrons situated on different centers). It takes the following form:

$$H = \sum_{i,\sigma} \alpha_i c_{i\sigma}^{\dagger} c_{i\sigma} + \sum_{i,j} t_{ij} \sum_{\sigma} (c_{i\sigma}^{\dagger} c_{j\sigma} + c_{j\sigma}^{\dagger} c_{i\sigma}) + \sum_{i} U_i n_{i\uparrow} n_{i\downarrow} + \sum_{i \neq j} V_{ij} n_i n_j \quad (1)$$

where i and j run over the considered orbitals and σ runs over the projection of the electron spin; $c_{i\sigma}^{\dagger}$ (or $c_{i\sigma}$) is the usual creation (or annihilation) operator of an electron of spin σ on site i; $n_{i\uparrow}$ (or $n_{i\downarrow}$) is the number operator of electron of spin α (or β) on site i; $n_i = n_{i\uparrow} + n_{i\downarrow}$ is the number operator of electrons on site i. The parameter α_i corresponds to the energy of the orbital i, t_{ij} to the hopping integral of an electron between sites i and j, U_i to the on-site effective electrostatic repulsion between two electrons on site i and V_{ij} to the inter-site effective electrostatic repulsion between two electrons on site i and j. In idealized Keggin compound as well as in the real structure of the particular salt studied in this work[17] all the W ions are equivalent. Then, all the d_{xy}-like orbitals of the W ions (the d orbital pointing between the equatorial O ions of the octahedron) considered in the model Hamiltonian are equivalent. Thus, α_i and U_i are identical for all the orbitals, the term $\alpha_i c_{i\sigma}^{\dagger} c_{i\sigma}$ acts as a reference for all the states and thus will not be taken into account in this work. In the case of strongly correlated systems, that is for systems where the U parameter is much greater than the t parameters, an important reduction of the model space is possible. Indeed, for half-filled systems, the high value of U allows to take into account only the forms with one electron per atomic orbital, leading to a spin model Hamiltonian. The effects of the determinants with double occupancy are taken into account in the effective value of J, the magnetic coupling parameter. For systems with one magnetic orbital per metal center a second order perturbative derivation of the Hubbard Hamiltonian leads to the famous Heisenberg–Dirac–van Vleck[5] model Hamiltonian:

$$H = -\sum_{i,j} J_{ij} \vec{S}_i \cdot \vec{S}_j \quad (2)$$

where is the local spin operator on site i; J_{ij} is the magnetic exchange integral between sites i and j. The sum over i,j is usually restricted to nearest-neighbors magnetic sites, *nn*, and eventually to next-nearest-neighbours, *nnn*. In the case of hole-doped magnetic systems (less than half-filled), the high value of U allows to limit the model space to determinants involving zero or one electron per atomic orbital (or, symmetrically, to determinants involving only one or two electrons per atomic orbital in the more than half filled electron-doped magnetic systems). It affords the t–J model[6] that considers both the magnetic coupling and electron transfer, or, when the inter-site electrostatic repulsion is important, to the t–J–V model Hamiltonian written as (see Equations (1) and (3) for notations):

$$H = \sum_{\langle i,j \rangle} t_{ij} \sum_{\sigma} (c_{i\sigma}^{\dagger} c_{j\sigma} + c_{j\sigma}^{\dagger} c_{i\sigma}) - \sum_{\langle i,j \rangle} J_{ij} \vec{S}_i \vec{S}_j + \sum_{i \neq j} V_{ij} n_i n_j \quad (3)$$

The exchange transfer (**e**) parameter[18] has to be introduced in systems based at least on three centers when the number of electrons is greater than one and different from the number of magnetic orbitals (doped-system). It corresponds to a three-center effective parameter originated, as the magnetic coupling, from the interactions between the configurations with zero or one electron per orbital with the determinants with two electrons in the same atomic orbital. Considering three atomic orbitals i, j and k, the e between orbitals i and j through k corresponds to the following pathways:

$$|i\bar{k}\rangle \leftrightarrow |k\bar{k}\rangle \leftrightarrow |j\bar{k}\rangle \text{ and}$$

$$|i\bar{k}\rangle \leftrightarrow |k\bar{k}\rangle \leftrightarrow |k\bar{j}\rangle$$

involving the Slater determinants $|i\bar{k}\rangle$ (an α electron in orbital i and a β electron in orbital k), $|j\bar{k}\rangle$ and $|k\bar{j}\rangle$ of the model space and the $|k\bar{k}\rangle$ doubly occupied determinant of the outer-space. The first pathway acts as an additional term to the effective electron transfer between orbitals i and j whereas the second term consists of the transfer of an electron between orbitals i and j with a simultaneous spin exchange with the electron of orbital k. These interactions are evidently possible only for two electrons of opposite spins. As a consequence, in a system containing only two delocalized electrons, the e has no effects on states with $S_z = 1$ and only acts on the singlet states. A "t–J–V–e" model Hamiltonian (a t–J–V model Hamiltonian to which is added the exchange-transfer parameter) is used to represent the system formed by two electrons delocalized on the d_{xy}-like orbitals of 4W ions. The hermitic matrix representative of this model Hamiltonian in the space of $S_z = 0$ is presented in Table 1. Tables 2 and 3 represent this model in a base of configurations adapted to the spatial symmetry and spin multiplicity.

An effective Hamiltonian procedure[19–21] was used to extract the values of the parameters of this model Hamiltonian. The effective Hamiltonian satisfies the two following properties: its eigenvalues are the eigenvalues of the exact Hamiltonian; its eigenvectors are the projections of the eigenvectors of the exact Hamiltonian into the effective space, the space handled by the effective Hamiltonian.

In the present case, the eigenvalues and eigenvectors of the "exact" Hamiltonian are those calculated with ab initio methods and the effective space contains all the determinants with zero or one electron per magnetic orbital. The result of this procedure is a matrix representative of the effective Hamiltonian. We use the Bloch formulation[19] that provides non-hermitic effective Hamiltonian matrices. The identification of its elements with the elements of the matrix representative of the model Hamiltonian directly provides the value of all the parameters. This method requires both the energies and the wave functions of all the states with the largest projection onto the effective space. For the three other systems (one electron delocalized over the 2W or 4W based fragments, and two electrons delocalized on the 2W based fragments) the same approach leads to much simpler formulations. Indeed, the extraction of the parameters is given by energy differences. A system of one electron delo-

Table 1. t–J–V–e model Hamiltonian for the 4W-based system with two delocalized electrons. a, b, c and d are the d_{xy}-like magnetic orbitals of the W_1, W_2, W_3 and W_4, respectively. $\langle a\bar{b}|$ is the Slater determinant corresponding to an electron of spin α in orbital a and an electrons of spin β in orbital b. Parameter e, e' and e^d correspond to the exchange transfer parameters. Notations te, te' and te^d stand for t+e, t'+e' and t^d+e^d, respectively. Parameters t, J, e and V correspond to interactions between corner-sharing WO_6 octahedra, t', J', e' and V' to interactions between edge-sharing octahedra and t^d, J^d, e^d and V^d to interactions between next-nearest-neighbors octahedra.

	$\lvert a\bar{c}\rangle$	$c\bar{a}\rangle$	$\lvert b\bar{d}\rangle$	$\lvert d\bar{b}\rangle$	$\lvert a\bar{d}\rangle$	$d\bar{a}\rangle$	$\lvert b\bar{c}\rangle$	$c\bar{b}\rangle$	$\lvert a\bar{b}\rangle$	$\lvert b\bar{a}\rangle$	$c\bar{d}\rangle$	$\lvert d\bar{c}\rangle$
$\langle a\bar{c}\rvert$	V^d	$J^d/2$	0	0	te'	e'	te'	e'	te	e	e	te
$\langle c\bar{a}\rvert$	$J^d/2$	V^d	0	0	e'	te'	e'	te'	e	te	te	e
$\langle b\bar{d}\rvert$	0	0	V^d	$J^d/2$	te'	e'	te'	e'	e	te	te	e
$\langle d\bar{b}\rvert$	0	0	$J^d/2$	V^d	e'	te'	e'	te'	te	e	e	te
$\langle a\bar{d}\rvert$	te'	e'	te'	e'	V	$J'/2$	0	0	te^d	e^d	te^d	e^d
$\langle d\bar{a}\rvert$	e'	te'	e'	te'	$J'/2$	V	0	0	e^d	te^d	e^d	te^d
$\langle b\bar{c}\rvert$	te'	e'	te'	e'	0	0	V	$J'/2$	e^d	te^d	e^d	te^d
$\langle c\bar{b}\rvert$	e'	te'	e'	te'	0	0	$J'/2$	V	te^d	e^d	te^d	e^d
$\langle a\bar{b}\rvert$	te	e	e	te	te^d	e^d	e^d	te^d	V'	$J/2$	0	0
$\langle b\bar{a}\rvert$	e	te	te	e	e^d	te^d	te^d	e^d	$J/2$	V'	0	0
$\langle c\bar{d}\rvert$	e	te	te	e	te^d	e^d	e^d	te^d	0	0	V'	$J/2$
$\langle d\bar{c}\rvert$	te	e	e	te	e^d	te^d	te^d	e^d	0	0	$J/2$	V'

Table 2. Hermitic matrices representative of the singlet configurations of the t–J–V–e model Hamiltonian for the 4W-based system. Ψ_1 = 1/2 ($a\bar{c}$+$c\bar{a}$+$b\bar{d}$+$d\bar{b}$), Ψ_2 = 1/2 ($a\bar{d}$+$d\bar{a}$+$b\bar{c}$+$c\bar{b}$), Ψ_3 = 1/2 ($a\bar{b}$+$b\bar{a}$+$c\bar{d}$+$d\bar{c}$), Ψ_4 = 1/2 ($a\bar{d}$+$d\bar{a}$−$b\bar{c}$−$c\bar{b}$), Ψ_5 = 1/2 ($a\bar{b}$+$b\bar{a}$−$c\bar{d}$−$d\bar{c}$), Ψ_6 = 1/2 ($a\bar{c}$+$c\bar{a}$−$b\bar{d}$−$d\bar{b}$).

	Ψ_1	Ψ_2	Ψ_3	Ψ_4	Ψ_5	Ψ_6
Ψ_1	V^d+$J^d/2$	$2t'$+$4e'$	$2t$+$4e$	0	0	0
Ψ_2	$2t'$+$4e'$	V+$J/2$	$2t^d$+$4e^d$	0	0	0
Ψ_3	$2t$+$4e$	$2t^d$+$4e^d$	V'+$J'/2$	0	0	0
Ψ_4	0	0	0	V+$J/2$	0	0
Ψ_5	0	0	0	0	V'+$J'/2$	0
Ψ_6	0	0	0	0	0	V^d+$J^d/2$

Table 3. Hermitic matrices representative of the triplet configurations of the t–J–V–e model Hamiltonian for the 4W-based system. Ψ_7 = 1/2 ($a\bar{c}$−$c\bar{a}$−$b\bar{d}$+$d\bar{b}$), Ψ_8 = 1/2 ($a\bar{b}$−$b\bar{a}$−$c\bar{d}$+$d\bar{c}$), Ψ_9 = 1/2 ($a\bar{c}$−$c\bar{a}$+$b\bar{d}$−$d\bar{b}$), Ψ_{10} = 1/2 ($a\bar{d}$−$d\bar{a}$+$b\bar{c}$−$c\bar{b}$), Ψ_{11} = 1/2 ($a\bar{d}$−$d\bar{a}$−$b\bar{c}$+$c\bar{b}$), Ψ_{12} = 1/2 ($a\bar{b}$−$b\bar{a}$+$c\bar{d}$−$d\bar{c}$).

	Ψ_7	Ψ_8	Ψ_9	Ψ_{10}	Ψ_{11}	Ψ_{12}
Ψ_7	V^d−$J^d/2$	$2t$	0	0	0	0
Ψ_8	$2t$	V'−$J'/2$	0	0	0	0
Ψ_9	0	0	V^d−$J^d/2$	$2t'$	0	0
Ψ_{10}	0	0	$2t'$	V−$J/2$	0	0
Ψ_{11}	0	0	0	0	V−$J/2$	$2t^d$
Ψ_{12}	0	0	0	0	$2t^d$	V'−$J'/2$

calized over four metal centers supports four doublets states D1, D2, D3 and D4 which wave functions are:

$$\Psi_{D1} = \frac{|a\rangle + |b\rangle + |c\rangle + |d\rangle}{2}$$

$$\Psi_{D2} = \frac{|a\rangle - |b\rangle - |c\rangle + |d\rangle}{2}$$

$$\Psi_{D3} = \frac{|a\rangle + |b\rangle - |c\rangle - |d\rangle}{2}$$

$$\Psi_{D4} = \frac{|a\rangle - |b\rangle + |c\rangle - |d\rangle}{2}$$

where $|a\rangle$, $|b\rangle$, $|c\rangle$ and $|d\rangle$ stand for the Slater determinants constructed when the extra electron is on W_1, W_2, W_3 or W_4, respectively (see Figure 2 for the numbering of the metal centers). The relations between the t, t', and t^d electron transfer parameters and the three energy gaps between the four doublet states are:

$$\begin{aligned} E_{12} &= E_2 - E_1 = -2t' - 2t^d \\ E_{13} &= E_3 - E_1 = -2t - 2t^d \\ E_{14} &= E_4 - E_1 = -2t - 2t' \end{aligned} \quad (4)$$

where E_1, E_2, E_3 and E_4 correspond to the energies of D1, D2, D3 and D4, respectively. These relations permit to determine t, t', and t^d parameters from the calculated energies. In the case of the delocalization of one electron over a 2W-based fragment the transfer parameter is related to the energy gap by the equation:

$$2t^i = E_{DD} = E_{D+} - E_{D-} \quad (5)$$

where t^i stands for t, t' or t^d depending on the fragment we are dealing with. E_{D+} and E_{D-} are the energies of the doublet states Ψ_{D+} and Ψ_{D-}, respectively. The symmetry of these two functions are those of d_1+d_2 and d_1−d_2, d_1 and d_2 standing for orbitals a, b, c or d. Thus, for the W_2O_9 fragments Ψ_{D+} is the antisymmetric doublet and Ψ_{D-} is the symmetric one, whereas in the W_2O_{10} fragment Ψ_{D+} is the symmetric doublet and Ψ_{D-} is the antisymmetric one.

In the case of calculations on systems with two electrons delocalized over two metal centers, the magnetic coupling is related to the difference:

$$J = E_{ST} = E_S - E_T \quad (6)$$

between the energies E_S and E_T of the singlet and triplet states. The difference between the on-site electrostatic repulsion U and the electrostatic repulsion between two different sites is given by the difference:

$$U-V = E_{S*} - E_T \quad (7)$$

between the energy E_{S*} of the singlet excited state essentially based on the configuration $|a\bar{a}\rangle - |b\bar{b}\rangle$ and the energy E_T

of the lowest triplet state essentially based on $|a\bar{b}\rangle - |b\bar{a}\rangle$. In conclusion, the processing of the energy and wave functions of the low energy states of the embedded fragments allow the evaluation of the parameters of the model Hamiltonian suited to represent the behavior of the whole Keggin anion.

Results and Discussion

Two electrons–4W-based system: The values for the magnetic coupling, electron transfer, exchange-transfer, and electrostatic repulsion parameters extracted from ab initio calculations on the system based on two electrons delocalized over the 4W fragment are listed in Table 4. The DDCI calculations are the most accurate ones (computational details are described in Computational Details). The two slightly different values of the t, t', e, and e' parameters are due to the non-hermiticity of the effective Hamiltonian, t^d and e^d are quasi-hermitic and the other parameters are hermitic. In any case, the intensity of the four-body terms ($\langle a\bar{c}|H|b\bar{d}\rangle$ for example) remain smaller than 10 meV. Because of the nature of the two electrons–4W-based system, it is not possible to extract independently V, V' and V^d. However, as it is very interesting to raise this constraint, the calculations on dimers presented in the next subsections fulfil this goal.

Table 4. Values in meV of the parameters of the t–J–V–e model extracted from calculations involving two electrons delocalized over the 4W-based fragment. P.C. are punctual charges calculations.

	t	t'	t^d	J	J'	J^d	e	e'	e^d	$V'-V$	$V'-V^d$
P.C.	–	–	–	–	–	–	–	–	–	+320	+1340
CASCI	−515	−531	−116	−81	−109	+20	−1/+1	−1/+3	−49	+204	+1388
MONO	−451/−462	−470/−479	−104	−140	−164	−0.7	−4/+12	−3/+11	−53	−5	+764
DDCI2	−461/−475	−485/−500	−116	−152	−183	+0.4	−5/+14	−4/+13	−53	+18	+756
DDCI	−490/−503	−509/−522	−154	−151	−190	+2.1	−8/+16	−5/+16	−67	+65	+854

The results show that the transfer parameters between corner-sharing or edge-sharing octahedra, t and t' parameters are of the same order, about −500 meV, while that between *nnn* octahedra, t^d, is 3–4 times smaller and of the same sign, whatever the level of calculation. The dynamical polarization (the difference between the MONO and CASCI results) provides a small positive contribution to the electron transfer parameters (about 10% of the CASCI value) whereas the other dynamical effects have small negative contributions. The magnetic couplings between metal centers belonging to edge-sharing and corner-sharing WO_6 octahedra, J and J', are strongly antiferromagnetic, about −150 and −190 meV, respectively. The magnetic coupling between *nnn* metal centers, J^d, is negligible (the ferromagnetic character of the J^d magnetic coupling at the CASCI level is due to the choice of the set of orbitals and the dynamical contributions compensate this effect). The exchange transfer parameter between *nnn* W centers, e^d, is large and is only slightly affected by the dynamical contributions. The e and e' parameters are smaller and strongly affected by the non-hermiticity of the Hamiltonian and by the dynamical contributions. The electrostatic repulsions along edge-sharing (V') and corner-sharing octahedra (V) significantly differ at the CASCI level but are almost equal at more accurate levels of calculations. A point charge evaluation of the electrostatic repulsion parameters from the distances $d_{III} = 5.2$, $d_{IV} = 3.8$, and $d_V = 3.5$ Å between the W ions gives $V^d = V_{III} \approx 2770$ meV, $V = V_{IV} \approx 3790$ meV and $V' = V_V \approx 4110$ meV, that is $V' - V \approx 320$ meV and $V' - V^d \approx 1340$ meV. These values are similar to those extracted from CASCI calculations, 204 and 1388 meV, respectively. But the important role of the dynamical effects makes these evaluations too simple to be accurate. A deeper analysis based on simple considerations of the structure of the Keggin anion would explain why the screening between W belonging to edge-sharing octahedra is stronger than that between W belonging to corner-sharing or *nnn* octahedra.

A second-order perturbative evaluation of the exchange transfer parameters permits to check the coherency of the results. Due to the non-hermiticity of the effective Hamiltonian, the perturbative evaluation gives two relations for each parameter:

$$e = -2\frac{t' \cdot t^d}{U - V'} \text{ and } e = -2\frac{t' \cdot t^d}{U - V^d}$$

$$e' = -2\frac{t \cdot t^d}{U - V} \text{ and } e' = -2\frac{t \cdot t^d}{U - V^d}$$

$$e^d = -2\frac{t \cdot t'}{U - V'} \text{ and } e^d = -2\frac{t \cdot t'}{U - V}$$

where the potential exchange transfer $\langle ab|H|ca\rangle$, $\langle ac|H|da\rangle$ and $\langle ab|H|da\rangle$ are neglected. These equations explain why e^d is quasi-hermitic ($V \approx V'$, which means that the denominators of the equations concerning e^d are almost equal) whereas e and e' are strongly non-hermitic ($V - V^d \approx V' - V^d \approx 0.8$ eV, thus the denominators of their equations significantly differ). But this perturbative development is too rough to explain the changes of the sign of e and e' reported in Table 4 and the potential exchange transfer parameters should be taken into account. If we consider that the differences between V, V' and V^d are small compared with the differences with U, all the denominators of all above relations are equal and the differences between the exchange transfer parameters arise from the numerators ($e \propto \{t' \cdot t^d\}$, $e' \propto \{t \cdot t^d\}$, and $e^d \propto \{t \cdot t'\}$). The ratio of about 3–4 between t or t' and t^d explains why e^d is much larger than the two other exchange transfer parameters. Furthermore, assuming that $V \approx V'$ and $t \approx t'$ in the evaluation of e^d, one obtains:

$$e^{d} \approx -2\frac{t^2}{U-V} \approx -2\frac{t'^2}{U-V'}$$

Comparing this relation to the usual estimation of the Anderson mechanisms[22] of the magnetic coupling parameters:

$$J = -\frac{4t^2}{U-V}$$

$$J' = -\frac{4t'^2}{U-V'}$$

one obtains $e^{d} \approx J/2 \approx J'/2$ that is coherent with the values reported in Table 4. Finally, it is important to point out that the values of e and e' cannot be accurately estimated by calculations on the chosen 4W-based fragment. Indeed, the main contributions for e and e' come from interactions with atoms out of the fragment (the third W atoms of the triads) that can be perturbatively estimated to:

$$e = -2\frac{t^2}{U-V} \text{ and}$$

$$e' = -2\frac{tt'^2}{U-V'}$$

Thus, e and e' should have values similar to e^{d}, that is $e \approx e' \approx e^{d} \approx -70$ meV.

Comparisons between results obtained from calculations on W_2O_9, W_2O_{10} and W_4O_{16} fragments: The interest of the 2W-based systems arise from the possibility not only to perform much quicker calculations than the one on the 4W-based systems, but also to better understand the electronic interactions occurring in these clusters by answering the following questions: How the transfer of a delocalized electron is affected by the presence of a second delocalized electron? Are the interactions local? Furthermore, even if it is usually assumed that embedded fragment calculations provide very accurate values of the electron transfer and magnetic coupling parameters, the present section is also devoted to check the accuracy of these calculations: Are dimers large enough? Are the TIPs and punctual charges adapted to reproduce the effects of the crystal on the fragment?

Table 5 summarizes the evaluations of the electron transfer and magnetic coupling parameters from calculations on the W_2O_9, W_2O_{10}, and W_4O_{16} with one or two delocalized electrons. As for the system containing two delocalized electrons, the DDCI calculations on the system based on one electron delocalized over four metal centers are performed on a restricted set of dedicated orbitals (see Computational Details).

Whatever the level of calculations, the values extracted for the parameters t, t', J and J' are not significantly affected, neither by the number of delocalized electrons, nor by the size of the fragment. We argue that the differences obtained for J' at the CASCI or CASSCF level on the 2W- and 4W-based fragments are just a consequence of the choice of the set of MOs. Some important consequences of these results have to be emphasized:

Table 5. Comparison of the values [meV] of the electron transfer and super-exchange parameters extracted from the calculations on the 4W-based fragment and on the three dimeric fragments with one or two delocalized electrons.

	System	t	t'	t^{d}	J	J'	J^{d}
CASCI	$2e^-/4W$	−515	−531	−116	−81	−109	+21
CASSCF	$2e^-/2W$	–	–	–	−79	−93	−0.7
CASSCF	$1e^-/4W$	−510	−551	−89	–	–	–
CASSCF	$1e^-/2W$	−510	−560	−80	–	–	–
CASPT2	$2e^-/2W$	–	–	–	−171	−208	−2.2
CASPT2	$1e^-/4W$	−443	−479	−125	–	–	–
CASPT2	$1e^-/2W$	−445	−490	−102	–	–	–
DDCI	$2e^-/4W$	−490/−503	−509/−522	−154	−151	−190	+2.1
DDCI	$2e^-/2W$	–	–	–	−178	−219	−3.2
DDCI	$1e^-/4W$	−504	−542	−140	–	–	–
DDCI	$1e^-/2W$	−467	−507		–	–	–

- the atoms that pertain to the 4W-based fragment but not to the 2W-based fragments are properly modeled by TIPs and punctual charges in the 2W-based calculations. The stability of the electron transfer and magnetic coupling parameters when the size of the fragments is changed means that punctual charges and TIPs reproduce accurately the effects of the ions outside those fragments.
- the 4W-based fragment allows to consider the effect of single and double excitations on ions that do not belong to the centers involved in the interaction process (for example, the excitation of an electron from a closed shell on the W_4 ion to its apical oxygen during the electron transfer between W_1 and W_2). This kind of "secondary" excitations are not possible in the 2W-based fragment. Thus, the similar values between the parameters derived from the 2W and 4W fragments prove that electron transfers and super-exchange are local phenomena (i.e., they essentially imply the two metal centers involved in the interaction and the oxygen ions of their coordination spheres, the electrons of the rest of the crystal only having an averaged influence).
- the transfer of a delocalized electron is not significantly affected by the presence of another delocalized electron on a neighbor center.
- the evaluation of the magnetic coupling between two electrons is very similar when the electrons are forced to pertain to a dimer or when they are allowed to delocalized over the 4W-based fragment.

On the contrary, the evaluation of t^{d} or J^{d} are more sensitive to the choice of the fragment. It is not a consequence of any physical effect but of the construction of the 2W-based fragment. Indeed, whereas in the fragment based on edge and corner-sharing octahedra all the nearest-neighbors atoms of the bridging oxygen are in the fragment, in the fragment based on *nnn* octahedra this is not the case (see Figure 3). That is why the W_2O_{10} fragment does not provide accurate values of the *nnn* electron transfer or magnetic coupling, and it is useless to perform DDCI calculations on

this model. Anyway, all calculations agree to predict a quite important electron transfer between *nnn* W ions.

Calculation of the electrostatic repulsions: Table 6 presents the evaluation of the difference between the on-site electrostatic repulsion (identical for all the metal centers which are symmetrically equivalent), and the electrostatic repulsion between two centers. The calculations are performed on the system based on two electrons delocalized over two metal centers at the CASSCF, CASPT2 and DDCI levels.

Table 6. Values [meV] of the electrostatic repulsion parameters extracted from calculations for *nn* W ions based fragments. The CASCI and DDCI calculations are performed on the set of orbitals optimized for the triplet state. P.C. are punctual charge calculations.

	$U-V'$	$V'-V$
P.C.	–	320
CASSCF	4922	379
CASPT2	4214	102
DDCI	3629	−8

The electrostatic effective repulsion parameters V and V' slightly differ at the CASSCF level. This difference is very similar to that obtained using a point charge evaluation (320 meV). At the DDCI level, V and V' are almost equal, in very good agreement with the values extracted from calculations on the 4W-based fragment. The two PW_2O_{14} fragments formed by the PO_4 clathrate and the WO_6 octahedra corresponding to the W ions farthest pairs (distances $d_{II}=$ 6.3 and $d_I=7.3$ Å) should permit an evaluation of the coulombic repulsion $U-V_{II}$ and $U-V_I$ from Equation (7). DDCI calculations performed on a dedicated set of MOs gives $U-V_I=6265$ meV, a result that does not change significantly with the choice of the set of MOs. However, convergence problems in the RASSCF procedure did not permit to obtain information about $U-V_{II}$. A very rough evaluation of V_{II} from point charge calculations gives $V_{II}-V_I \approx 0.3$ eV. A combination of the values of all the electrostatic repulsion parameters permits to draw the scheme of energy differences between V_I, V_{II}, V_{III}, V_{IV}, and V_V represented in Figure 4.

Conclusion on the ab initio calculations part: As a conclusion on the ab initio calculations part, we have shown how the punctual charges and TIPs are suited to model the effects on the considered fragments of the rest of the crystal. We have also proven that dimer fragment calculations permit an accurate evaluation of the t, t', J, J', V, V'. We can also reasonably assume that the on-site electrostatic effective repulsion is accurately calculated on these fragments. However, calculations on 4W-based fragments are necessary to get reasonable values for t^d, J^d and V^d.

A Model Hamiltonian for the whole Keggin anion

This section is devoted to understand the origin of the diamagnetic properties of the two-electron reduced Keggin polyoxoanion. For this purpose, we used the model Hamiltonian

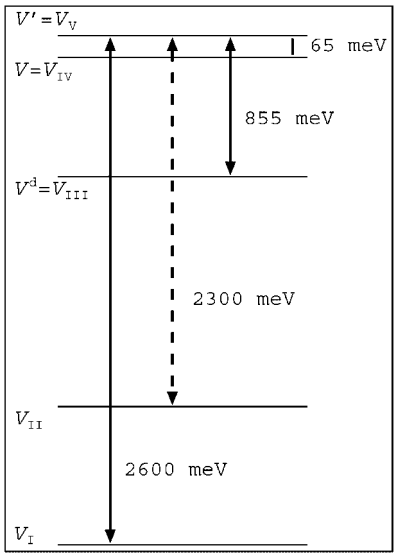

Figure 4. Scheme of the differences between the inter-site electrostatic repulsion. Energy differences represented by plain arrows are obtained from ab initio calculations and are quite accurate. The energy difference represented by dashed arrows is a rough estimation obtained from punctual charges calculations.

proposed in ref. [23] which describes the behavior of the whole Keggin anion reduced by two electrons. This Hamiltonian is based on a chain-like spin coupling scheme that represents the interactions between two spins delocalized over 12 magnetic centers. It takes into account all the parameters described in the Section on Model Hamiltonians and evaluation of their parameters. The energies of the Hamiltonian, obtained from an exact diagonalization of the corresponding matrices, can be compared with the energies that could be measured on a two-electron-reduced Keggin anion. The use of the ab initio value of all the microscopic parameters permits to evaluate the energy gap between the singlet ground state and the lowest triplet state. It is about 0.8 eV. This very large value prevent any significant thermal population of the triplet state even at room temperature. Our results are in complete agreement with the diamagnetic properties of the two electron reduced Keggin anions. Nevertheless, the origin of this very large energy gap has to be explained as strong electrostatic repulsions maintain the delocalized "extra" electrons far one from each other. In order to discriminate the influence of each kind of microscopic parameters onto the singlet-to-triplet gap, they are included step by step in the model Hamiltonian and the energy of the lowest states are extracted. The changes of the singlet-to-triplet energy gap when a parameter is taken into account or not permits to evaluate its importance on the diamagnetic properties of the material.

Influence of electrostatic repulsion: The large value of the V_V, V_{IV}, V_{III} electrostatic repulsions versus V_{II} and V_I permits to draw a very simple model Hamiltonian. It is built from configurations based on two electrons separated by distances d_I or d_{II}. Super-exchange mechanisms between W centers separated by distances d_I or d_{II} are almost zero and the other parameters of such a model are the electron transfer

between nearest-neighbors metal centers (t and t'). The diagonalization of the model Hamiltonian using the values extracted in this work ($V_{II} - V_I = 0.3$ eV, $t = t' = 0.5\,eV$) predicts an singlet-to-triplet energy gap of 0.3 eV. Thus, this simple model contains about 40% of the mechanisms responsible of the magnetic coupling between the two delocalized electrons. The next step is to check the importance of the very poor accuracy of the evaluation of V_I and V_{II}. For that purpose, the V_V, V_{IV}, V_{III} parameters are introduced in the model whereas t^d, J, J' and J^d remain neglected (their effects is checked in the next subsections) and $t = t' = 0.5\,eV$. The variations of the gap with the values of V_I and V_{II} are evaluated from two series of calculations:

- in Figure 5, V_I, V_{III}, V_{IV} and V_V are fixed to the calculated values and V_{II} varies from V_I to V_{III};
- in Figure 6, V_{III}, V_{IV} and V_V are fixed to the calculated values, the ratio $V_{III} - V_{II}/V_{II} - V_I$ is kept constant and the differences $V_{II} - V_I$ varies from 0 (i.e., $V_I = V_{II} = V_{III}$) to $V_{II} - V_I = |t| \approx 500$ meV, a value about 1.6 times larger than the ab initio one.

The evolution of the low lying levels shows that in a wide range of V_I and V_{II} values, the singlet-to-triplet energy gap is very large. This gap is unchanged whatever the value of V_{II} when V_I and V_{III} are kept constant (Figure 5). Simultaneous changes of V_{II} and V_I (Figure 6) slightly affect the singlet-to-triplet energy gap. It is increased by only 0.09 eV when $V_I = V_{II} = V_{III}$ versus the value assuming the calculated electrostatic repulsions $V_{II} - V_I = 0.3$ eV. Thus, the limited accuracy in the evaluation of V_I and V_{II} does not change the interpretation we can make about the origin of the diamagnetism in this mixed valence cluster. Taking into account all the electrostatic repulsion parameters, neglecting the super exchange mechanisms and td, the singlet-to-triplet energy gap is of 0.56 eV, a 70% of the actual value. Moreover, the configurations where the delocalized electrons are separated by distances d_{III}, d_{IV} or d_V should not be neglected as they contribute to about 30% to the total singlet-to-triplet energy gap.

Influence of diagonal transfer: The influence of the diagonal transfer parameter is evaluated by fixing t, t' and all the electrostatic repulsions to their ab initio values and calculating the low lying levels when t^d varies in a large range of values (see Figure 7). The value $t^d = 0$ corresponds to the assumptions made in the previous subsection, while the vertical dashed line corresponds to the value determined by ab initio methods. The singlet-to-triplet energy gap rapidly varies with t^d. For negative t^d this gap increases with the absolute value of t^d, while the reverse situation occurs for positive t^d values. For $t^d = -140$ meV, the gap is of 0.77 eV, a 40% larger than for $t^d = 0$, and a 96% of the actual value (when J and J' are not neglected).

Influence of exchange parameters: Finally, the influence of the exchange parameters on the effective coupling between the two delocalized electrons is reported in the correlation diagram shown in Figure 8. This plot represents the evolution of the lowest spin states of the Keggin anion with J and J' in the particular case where $J = J'$. The values of all the other parameters are those evaluated from ab initio calcula-

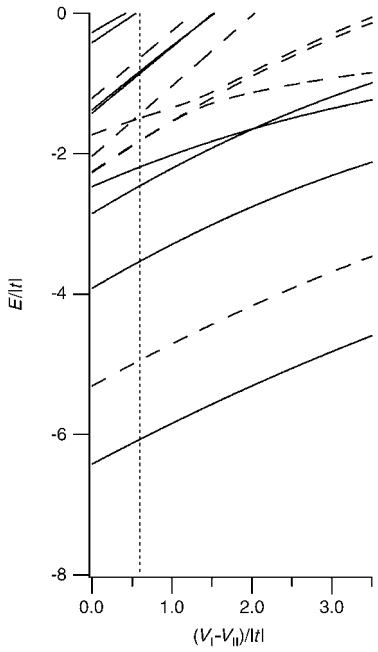

Figure 5. Evolution of the low lying energy levels with V_{II}. The values for t, t', V_I, V_{III}, V_{IV} and V_V are determined by ab initio calculations. t^d, J and J' are supposed to be 0. Solid lines correspond to singlet states, dashed lines to triplet states. The vertical dashed line corresponds to the value determined by ab initio methods.

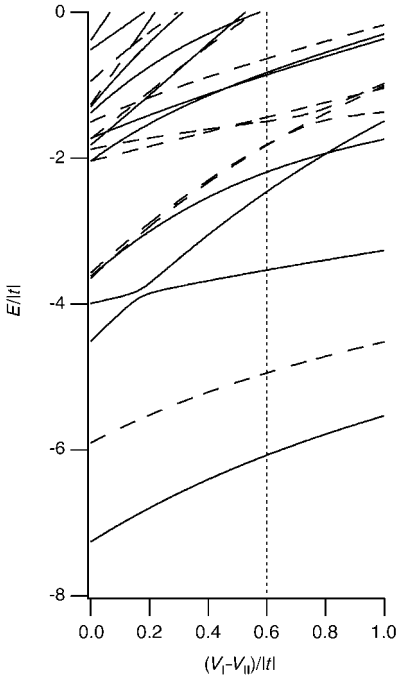

Figure 6. Evolution of the low lying levels with V_I and V_{II}. The values for t, t', $V_V - V_{III}$ and $V_{IV} - V_{III}$ are determined by ab initio calculations. t^d, J and J' are supposed to be 0. Solid lines correspond to singlet states, dashed lines to triplet states. The vertical dashed line corresponds to the value determined by ab initio methods.

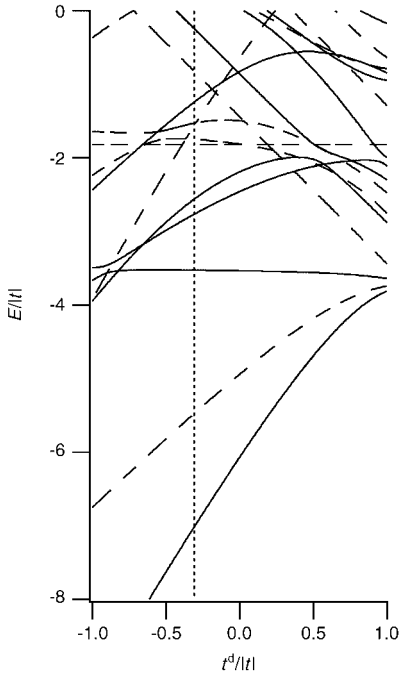

Figure 7. Evolution of the low lying levels with t^{d}. The values for t, t' and all the electrostatic repulsions are those obtained from ab initio calculations. J and J' are supposed to be 0. Solid lines correspond to singlet states, dashed lines to triplet states. The vertical dashed line corresponds to the value determined by ab initio methods.

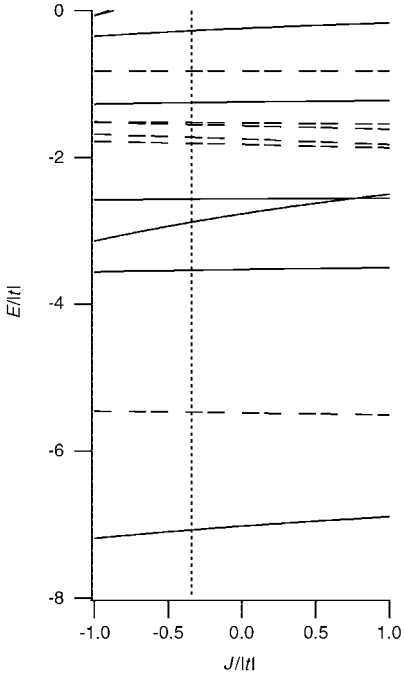

Figure 8. Evolution of the energy of the low lying energy levels with the exchange parameters. The value of t, t', t^{d} and all the electrostatic repulsions are those obtained from ab initio calculations. Solid lines correspond to singlet states, dashed lines to triplet states. The vertical dashed line corresponds to the value determined by ab initio methods.

tions. As expected an antiferromagnetic (negative) exchange interaction leads to an increase in the singlet-to-triplet energy gap. However, this effect is quite small. In our case, even if J and J' are strongly antiferromagnetic, the resulting gap only increases about 0.03 eV with respect to the value at $J = J' = 0$, to a total of 0.80 eV, the most accurate evaluation of this work. For a value of J as large as t this gap would be only increased by a 8% in the most favourable case $V_{V} \approx V_{IV}$.

Conclusions

The method used in this work provides for the first time a complete and definite explanation of the diamagnetic properties of these high nuclearity mixed-valence clusters. A singlet–triplet energy gap of 0.80 eV (6450 cm^{-1}) has been estimated. By combining an ab initio evaluation of the interactions between the electrons delocalized over the Keggin anion with the use of these parameters in a model Hamiltonian of the whole anion, it has been clearly proved that the diamagnetism of the two-electron reduced Keggin anion is essentially a consequence of the electron transfer processes occurring between the nearest W centers, and of the Coulombic repulsion between the delocalized electrons. Dealing with electron transfer, the major contributions arise from the edge-sharing and corner-sharing transfer parameters, t and t', although the presence of an unexpected quite large diagonal transfer, td, which involves next-nearest-neighbor interactions, affords an important additional mechanism to stabilize the singlet ground spin state. Additionally, it has been shown that the electrostatic Coulombic repulsion also plays a key role in the stabilization of the singlet ground spin state. In turn, it has been found that the contribution of a multiroute superexchange mechanism, that was initially invoked to explain the diamagnetism in these clusters, is quite negligible. The diamagnetism of two-electron reduced Keggin anion is explained by the solely evaluation of the very large singlet–triplet energy gap. However, the hybrid approach of this paper is general and useful for a better understanding of the magnetic properties of a large range of mixed-valence polyoxometalate compounds. Indeed, the parametrization of the Hubbard model Hamiltonian by the same set of microscopic interactions evaluated from ab initio methods has a much wider prediction capability which extends to magnetic susceptibility, magnetization, heat capacity or even inelastic neutron scattering experiments.

Computational Details

Ab initio methods: The physics of mixed-valence compounds permit to differentiate the orbitals into three sets following their contributions to the magnetic properties: i) the orbitals that are essentially closed shell orbitals; ii) the orbitals that essentially remain empty; iii) the magnetic orbitals. Following these distinctions, the complete active space self consistent field (CASSCF)[24] procedure defines three sets of orbitals: i) the inactive orbitals which are doubly occupied orbitals; ii) the virtual orbitals that are empty; iii) the active orbitals, whose occupations are allowed to change, support the active electrons. The complete active space (CAS) is then defined, for a given number of active electrons, as the set of all the determinants allowed by the previous occupation rules. For a state of a given spatial symmetry and spin multiplicity, the CASSCF procedure consists of the simultaneous self-consistent optimisation of all the molec-

ular orbitals (MOs) and of the coefficients of the wave function developed onto the CAS. It treats exactly the interactions between the active electrons in the mean field of the remaining electrons. That way, the static polarization and a small fraction of the correlation of the active electrons are *variationally* taken into account. This procedure can be extended to the "State Average CASSCF" procedure that consists in the optimisation of the wave functions of *various states* (of the same spatial symmetry and spin multiplicity) and of a *common* set of MOs. The complete active space configuration interaction (CASCI) procedure consists, for a *given* set of MOs, in the optimisation of the coefficients of the wave function of a state developed onto the CAS. The CASPT2[25] calculations permit a second-order perturbative evaluation of the dynamical polarisation and correlation effects. The MONO, DDCI2 and DDCI methods[26] are variational calculations of part of the dynamical effects. The MONO takes into account the dynamical polarisation of the determinants of the CAS. It is obtained by the diagonalization of the determinantal space containing the CAS and all the single excitations onto the CAS, corresponding to the following determinants: i) excitations inside the CAS; ii) one hole (one electron is excited from an inactive orbital to an active orbital); iii) one particle (one electron is excited from an active orbital to a virtual orbital); iv) one hole + one particle (one electron is excited from an inactive orbital to an active orbital and one electron is excited from an active orbital to a virtual orbital). The DDCI2 space adds to the previous space the double excitations involving utmost two inactive or virtual orbitals, that is two holes or two particles. Finally, the DDCI space includes the DDCI2 space and the following excitations: "two-holes + one-particle" and "one-hole + two-particles". The DDCI space includes all the determinants that participate, at a second-order of perturbation, to the energy differences between all the states of the CAS. Other contributions of these excitations appear at the third order of perturbation as polarization of the orbitals of the oxo ligands that allow the electron transfer from one metal to the other. The double excitations that do not belong to the DDCI space correspond to the "two-holes + two-particles" excitations. They are evidently the most numerous when the number of inactive and virtual orbitals is large compared with the number of active orbitals. At the second order of perturbation their effect is only to shift the energy of all the states of the CAS by the same quantity when a common set of MOs is used for the calculations of all the states. Thus, the DDCI procedure takes into account variationally the main differential dynamical effects and is the most accurate method used in this work. The last computational detail that has to be stressed concerns the selection of the inactive and virtual orbitals included in the calculations of the dynamical effects. Indeed, the occupied orbitals from which the excitations are originated, and the orbitals to which they end can be selected. This permits to neglect those excitations that are supposed to give the smallest contributions. The inactive (or virtual) orbitals that are not allowed to participate in the excitations are named frozen (or deleted) orbitals. For CASPT2 calculations, the selection is usually done taking into account an energetic criterion since a perturbative approach predicts that the higher the energy gap between the orbitals involved in the excitation is, the smaller the contribution to the wave function and the smaller the correction to the energy. For variational calculations, a method to select the frozen and deleted orbitals recently proposed[27] has proved its high efficiency. The criterion in this case is the difference of participation of the orbitals to the CI of the states: the inactive or virtual orbitals that are equivalently occupied in all states can be neglected whereas those whose occupation changes significantly have to be taken into account into the CI. The "energy difference dedicated orbitals" are obtained by the difference of the density matrices of the states calculated at the MONO level. See ref. [27] for more details. The CASSCF and CASPT2 are part of the MOLCAS suite of programs.[28] The MONO, DDCI2 and DDCI results are obtained with the CASDI code.[29]

The sets of MOs: For those systems formed by one or two electrons delocalized over the 2W-based fragments, the CASPT2 procedure is performed on the CASSCF set of orbitals. The MONO, DDCI2 and DDCI are performed on the set of orbitals optimized for the triplet state in the case of calculations involving two delocalized electrons, and on the set of MOs of the ground doublet state in the case of calculations involving only one delocalized electron. In any case, we check that the DDCI results obtained with different sets of MOs do not change significantly the values of the parameters. For the system formed by one electron delocalized over the 4W-based fragments, the CASPT2 calculations are performed on the set of MOs optimized for each of the doublet state at the CASSCF level. In the case of the system formed by two electrons delocalized over the 4W-based fragments, the CASCI calculations are performed on the set of MOs optimized at the State Average CASSCF level for the lowest singlet state and the two other singlet states of the same symmetry. The projections of these three states onto the CAS are combinations of the following configurations (see the first matrix of Table 2):

$$C_1 = \frac{a\bar{c} + c\bar{a} + b\bar{d} + d\bar{b}}{2}$$

$$C_2 = \frac{a\bar{b} + b\bar{a} + c\bar{d} + d\bar{c}}{2}$$

$$C_3 = \frac{a\bar{d} + d\bar{a} + b\bar{c} + c\bar{b}}{2}$$

These configurations exhibit the three kinds of electrostatic repulsion between the delocalized electrons (V^{d} for C_1, V' for C_2 and V for C_3). Thus, the set of orbitals optimized for these three states should be well suited to calculate all the states. Anyway, the DDCI procedure exhibit only a small dependency with the set of MOs. For technical reasons, the very large number (460) of orbitals of the system based on four tungsten centers prevents to perform any calculation with MONO, DDCI2 or DDCI methods. The CASPT2 method can handle such a large number of orbitals but accurate CASPT2 calculations need a CASSCF set of orbitals for each state. The extraction of parameters of the two-electrons–4W system is possible only if a common set of MOs is used for all the calculations. Thus, it is not possible to extract accurate values of the parameters of the two-electrons–4W system from CASPT2 calculations. Nevertheless, a combination of CASPT2 and DDCI methods can provide accurate evaluations of the parameters from calculations on the two-electrons–4W-based systems. The problem is to obtain a reduced set of orbitals that contains the main part of the dynamical effects and that permits DDCI calculations. This set of MOs is obtained with a two-step procedure: i) the first step consists of deletion a large number of virtual orbitals so that to be able to perform MONO calculations; ii) second, the calculation of the energy difference dedicated orbitals and the selection of a set of MOs that provides the main dynamical contributions and is small enough to permit the DDCI calculations. To check the effects of the rough simplifications introduced in the first step, the CASPT2 method is used. Indeed, even if accurate CASPT2 calculations impose the use of orbitals optimized for each state, a CASPT2 calculation on the same set of orbitals with a different number of deleted orbitals provides an evaluation of the dynamical energetic contribution of the deleted orbitals. Thus, two calculations are performed on the set of MOs optimized at the state average CASSCF level for the lowest singlet state and for the two other singlet states of the same symmetry: firstly, the reference where all the virtual orbitals are allowed to participate to the excitations is evaluated. A second calculation is performed on a reduced set of 248 MOs, where 212 virtual orbitals are deleted on an energetic criterion. The two resulting spectra are represented in Figure 9. They compare very well, proving the small participation of the deleted orbitals. Thus, the space of the single and double excitations based on the $460-212=248$ orbitals contains the main contributions to the energy differences between the states and accurate evaluations of the parameters can be expected from calculations on this reduced set of orbitals.

This reduced set of orbitals allows MONO and DDCI2 calculations to be performed, but still the DDCI space remains very large, about 25×10^6 determinants. Even if this calculation is not impossible, the use of a selected set of energy difference dedicated orbitals reduces the DDCI space by about 55% without any significant loss of precision on the values of the parameters as presented in Table 7. As we can see, the values of the parameters do not depend of the set of MOs; the error due to the use of the energy difference dedicated orbitals is almost zero for any kind of parameter.

The aim of the energy difference dedicated orbitals method is to concentrate the dynamical effects into a reduced set of orbitals. These MOs are obtained from MONO calculations. They are thus suited to reproduce the energy and wave functions of the states (and thus the parameters) ob-

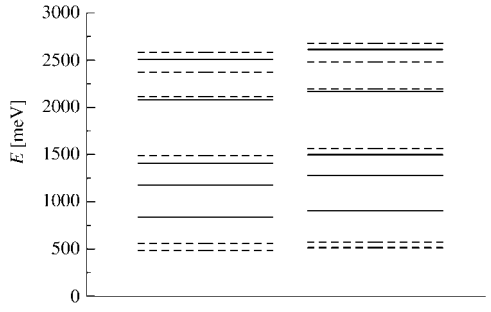

Figure 9. Spectrum obtained from CASPT2 calculations on the 4W-based fragment with two delocalized electrons. On the left, the spectrum obtained when all the virtual orbitals participate, on the right, the spectrum obtained when a large number (212) of orbital are deleted. The order of the states does not change. Solid lines correspond to singlet states, dashed lines to triplet states. The energy of the singlet ground state is taken as reference.

Table 7. Accuracy of calculations at MONO and DDCI2 levels, when 1) 248 MOs or 2) dedicated MOs are used. Values are in meV.

	t	t'	t^d	J	J'	J^d	e	e'	e^d	$V'-V$	$V'-V^d$
MONO(1)	−452/−463	−470/−480	−104	−141	−165	−0.8	−4/+12	−3/+12	−53	−2	760
MONO(2)	−451/−462	−470/−479	−104	−140	−164	−0.7	−4/+12	−3/+11	−53	−5	764
DDCI(1)	−461/−475	−485/−500	−117	−154	−185	−0.1	−5/+14	−4/+13	−53	+20	752
DDCI(2)	−461/−475	−485/−500	−116	−152	−183	+0.4	−5/+14	−4/+13	−53	+18	756

tained at the MONO level of calculations on the complete set of orbitals. However, it is interesting to notice that even if the DDCI2 space contains excitations out of the MONO space, the DDCI2 results on the selected dedicated orbitals and on the complete set of orbitals are very similar. The set of selected dedicated orbitals are well suited for both MONO and DDCI2 calculations and we can reasonably assume that they are also well suited for the DDCI calculations. Thus, we can trust in the DDCI values presented in Table 4.

Atomic basis sets: In all the calculations, the inner-core electrons ($[1s^2 2s^2 2p^6 3s^2 3p^6 4s^2 3d^{10} 4p^6 5s^2 4d^{10} 4f^{14}]$ for the W atoms and $[1s^2]$ for the O atoms) are represented by effective core potential (ECPs). The outer-core and valence electrons are represented using a 13s10p9d5f primitive basis set contracted to 3s3p4d2f for the W atoms, a 5s6p1d primitive basis set contracted to 2s4p1d for all the O atoms exempt for the apical oxygen atom for which the use of a stronger contraction to 1s2p1d was checked to have no significant effects. The exact expression of the basis sets and ECPs can be found in reference.[30]

Acknowledgement

This research was financially supported by the European Community (Network Molnanomag, no. HPRN-CT-1999-00012), by the spanish Ministerio de Ciencia y Tecnología (MAT2001-3507) and by the Generalitat Valenciana (GV01-312). A. Gaita-Ariño thanks the Generalitat Valenciana for a predoctoral grant. J. M. Clemente-Juan thanks the Spanish Ministerio de Ciencia y Tecnología for a "Ramón y Cajal" contract. We thank Marie-Bernadette Lepetit for many fruitful discussions, Carmen Jimenez-Calzado for helping us with the program of extraction of ab initio parameters, Daniel Maynau for the CASDI suite of programs and Alain Gelle for his program of localisation of orbitals. Part of the calculations were performed at IDRIS/CNRS under project number 1104.

[1] *Chem. Rev.* **1998**, *98*, whole issue; M. T. Pope, *Isopoly and Heteropoly Metalates*, Springer, Berlin, **1983**; M. T. Pope, A. Müller, *Polyoxometalates: from Platonic Solids to Anti-retroviral Activity*, Kluwer Academic, Dordrecht, **1994**; A. Müller, E. Krickemeyer, M. Penk, V. Wittneben, J. Döring, *Angew. Chem.* **1990**, *102*, 926; *Angew. Chem. Int. Ed. Eng.* **1990**, *29*, 926.
[2] I. Lindquist, *Ark. Kemi.* **1952**, *5*, 247; J. F. Keggin, *Nature* **1933**, *131*, 908; B. Dawson, *Acta Paediatr. Lat.* **2001**, *222*, 193.
[3] D. E. Katsoulis, *Chem. Rev.* **1998**, *98*, 359.
[4] M. Kozik, C. F. Hammer, L. C. W. Baker, *J. Am. Chem. Soc.* **1986**, *108*, 2748; M. Kozik, L. C. W. Baker, *J. Am. Chem. Soc.* **1987**, *109*, 3159; M. Kozik, N. Casan-Pastor, C. F. Hammer, L. C. W. Baker, *J. Am. Chem. Soc.* **1988**, *110*, 1697; M. Kozik, L. C. W. Baker, *J. Am. Chem. Soc.* **1990**, *112*, 7604; N. Casan-Pastor, L. C. W. Baker, *J. Am. Chem. Soc.* **1992**, *114*, 10384.
[5] W. Heisenberg, *Z. Phys.* **1928**, *49*, 619; P. A. M. Dirac, *Proc. R. Soc. London Ser. A* **1929**, *123*, 714; P. A. M. Dirac, in *The Principles of Quantum Mechanics*, Clarendon Press, Oxford, **1947**; J. H. Van Vleck, in *The Theory of Electric and Magnetic Susceptibilities*, Oxford University Press, Oxford, **1932**.
[6] P. W. Anderson, *Sciences* **1987**, *23*, 1196; C. Zhang, T. Rice, *Phys. Rev. B* **1988**, *37*, 3759.
[7] J. Hubbard, *Proc. R. Soc. London Ser. A* **1963**, *276*, 238; J. Hubbard, *Proc. R. Soc. London Ser. A* **1963**, *277*, 237; J. Hubbard, *Proc. R. Soc. London Ser. A* **1963**, *281*, 401.
[8] R. Pariser, R. G. Parr, *J. Chem. Phys.* **1953**, *21*, 466;R. Pariser, R. G. Parr, *J. Chem. Phys.* **1953**, *21*, 767; J. A. Pople, *Trans. Faraday Soc.* **1953**, *49*, 1375.
[9] H. Duclusaud, S. A. Borshch, *J. Am. Chem. Soc.* **2001**, *123*, 2825; J. M. Maestre, X. Lopez, C. Bo, J.-M. Poblet, N. Casan-Pastor, *J. Am. Chem. Soc.* **2001**, *123*, 3749; X. Lopez, J. M. Maestre, C. Bo, J.-M. Poblet, *J. Am. Chem. Soc.* **2001**, *123*, 9571; X. Lopez, C. Bo, J.-M. Poblet, *J. Am. Chem. Soc.* **2002**, *124*, 12574.
[10] N. Suaud, A. Gaita-Ariño, J. M. Clemente-Juan, J. Sánchez-Marín, E. Coronado, *J. Am. Chem. Soc.* **2002**, *124*, 15134.
[11] N. Suaud, M.-B. Lepetit, *Phys. Rev.* **2000**, *B62*, 402; N. Suaud, M.-B. Lepetit, *Phys. Rev. Lett.* **2002**, *88*, 056405.
[12] I. de P. R. Moreira, F. Illas, C. Jimenez-Calzado, J. Fernandez-Sanz, J. P. Malrieu, N. Ben Amor, D. Maynau, *Phys. Rev. B.* **1999**, *59*, 6593; C. Jimenez-Calzado, J. Fernandez-Sanz, J. P. Malrieu, F. Illas, *Chem. Phys. Lett.* **1999**, *307*, 102; D. Munoz, F. Illas, I. de P. R. Moreira, *Phys. Rev. Lett.* **2000**, *84*, 1579; C. Jimenez-Calzado, J. Fernandez-Sanz, J. P. Malrieu, *J. Chem. Phys.* **2000**, *112*, 5158; L. Hozoi, A. H. de Vries, A. B. van Oosten, R. Broer, J. Cabrero, C. de Graaf, *Phys. Rev. Lett.* **2002**, *89*, 076407.
[13] M. S. Hybersten, E. Stechel, B. M. Schluter, D. R. Jennison, *Phys. Rev. B* **1990**, *41*, 11068.
[14] P. Durand, J. C. Barthelat, *Theor. Chim. Acta* **1975**, *38*, 283.
[15] M.-B. Lepetit, N. Suaud, A. Gelle, V. Robert, *J. Chem. Phys.* **2003**, *118*, 3966.
[16] C. Jimenez-Calzado, A. Gaita-Ariño, N. Suaud, J. M. Clemente-Juan, E. Coronado, unpublished results.
[17] G. M. Brown, M.-RW. R. Noe-Spirlet, H. Busing, A. Levy, *Acta Crystallogr.* **1977**, *B33*, 1038.
[18] J. J. Girerd, V. K. Papaefthymiou, K. Surerus, E. Munck, *Pure Appl. Chem.* **1989**, *61*, 805; J. E. Hirsch, *Phys. Rev. Lett.* **1985**, *54*, 1317; J. J. Borrás-Almenar, E. Coronado, R. Georges, A. V. Palii, B. S. Tsukerblat, *Phys. Lett.* **1996**, *A220*, 342; J. J. Borrás-Almenar, E. Coronado, R. Georges, A. V. Palii, B. S. Tsukerblat *Chem. Phys. Lett.* **1996**, *249*, 7; J. J. Borrás-Almenar, E. Coronado, A. V. Palii, B. S. Tsukerblat, R. Georges, *Chem. Phys.* **1998**, *226*, 231.
[19] C. Bloch, *Nucl. Phys.* **1958**, *6*, 329.
[20] J. des Cloizeaux, *Nucl. Phys.* **1960**, *20*, 321.
[21] Program written by Carmen Jimenez-Calzado from the Universidad de Sevilla, Spain.
[22] P. W. Anderson, *Solid State Phys.* **1963**, *14*, 99.

[23] J. J. Borrás-Almenar, J. M. Clemente-Juan, E. Coronado, B. S. Tsukerblat, *Chem. Phys.* **1995**, *195*, 1; J. J. Borrás-Almenar, J. M. Clemente-Juan, E. Coronado, B. S. Tsukerblat, *Chem. Phys.* **1995**, *195*, 29.
[24] B. O. Roos, in *Advances in Chemical Physics; Ab Initio Methods in Quantum Chemistry - II* (Ed.: K. P. Lawley), Wiley, Chichester (UK), **1987**, p. 399; B. O. Roos, P. R. Taylor, P. E. M. Siegbahn, *Chem. Phys.* **1980**, *48*, 157.
[25] K. Andersson, P.-Å. Malmqvist, B. O. Roos, A. J. Sadlej, K. Wolinski, *J. Phys. Chem.* **1990**, *94*, 5483; K. Andersson, P.-Å. Malmqvist, B. O. Roos, *J. Chem. Phys.* **1992**, *96*, 1218.
[26] J. P. Malrieu, *J. Chem. Phys.* **1967**, *47*, 4555; R. Broer, W. J. A. Maaskant, *Chem. Phys.* **1986**, *102*, 103; J. Miralles, O. Castell, R. Caballol, J. P. Malrieu, *Chem. Phys.* **1993**, *172*, 33; J. Cabrero, N. Ben Amor, C. de Graaf, F. Illas, R. Caballol, *J. Phys. Chem.* **2000**, *A104*, 9983.
[27] C. Jimenez-Calzado, J. P. Malrieu, J. Cabrero, R. Caballol, *J. Chem. Phys.* **2000**, *104*, 11 636.
[28] MOLCAS Version 5.2, K. Andersson, M. Barysz, A. Bernhardsson, M. R. A. Blomberg, Y. Carissan, D. L. Cooper, M. Cossi, T. Fleig, M. P. Fülscher, L. Gagliardi, C. de Graaf, B. A. Hess, G. Karlström, R. Lindh, P.-Å. Malmqvist, P. Neogrády, J. Olsen, B. O. Roos, B. Schimmelpfennig, M. Schütz, L. Seijo, L. Serrano-Andrés, P. E. M. Siegbahn, J. Stålring, T. Thorsteinsson, V. Veryazov, M. Wierzbowska, P.-O. Widmark, Lund University (Sweden), **2001**.
[29] CASDI suite of programs, D. Maynau, N. Ben Amor, Pitarch-Ruiz, J. V. University of Toulouse (France), **1999**; N. Ben Amor, D. Maynau, *Chem. Phys. Lett.* **1998**, *286*, 211; J. V. Pitarch- Ruiz, J. Sánchez-Marín, D. Maynau, *J. Comput. Chem.* **2002**, *23*, 1157.
[30] Z. Barandiarán, L. Seijo, *Can. J. Chem.* **1992**, *70*, 409.

Received: October 16, 2003
Revised: March 10, 2004
Published online: June 30, 2004

